SOURCES AND DETECTION OF DARK MATTER AND DARK ENERGY IN THE UNIVERSE

Proceedings of the 8th UCLA Symposium

Marina del Rey, California 20–22 February 2008

EDITOR
David B. Cline
UCLA
Los Angeles, California

AMERICAN INSTITUTE OF PHYSICS

Melville, New York, 2009
AIP CONFERENCE PROCEEDINGS ▮ 1166

E-mail address of Dr. Klaus Volkamer: dr.volkamer@t-online.de

Gravitational Spacecraft Anomalies as well as the at Present Relatively large Uncertainty of Newton's Gravity Constant are Explained on the Basis of Force-Effects Due to a so-far Unknown Form of Space-like Matter

Klaus Volkamer

ISMR, Heidelberger Ring 21, D-67227 Frankenthal, Germany, dr.volkamer@t-online.de

Abstract. Recently, a so-far unkown form of invisible, space-like and field-like form of matter was detected with real, weighable mass content. The observed quanta of field-like matter exhibit in laboratory experiments Planck mass $m_P = \sqrt{\hbar \cdot c/G} = 21.77\,\mu g$. They show either a positive or negative sign, and can be understood as candidates for **dark matter** (field-like quanta with positive sign) and **dark energy** (field-like quanta with negative sign). Due to the observed gravitational as well as "topological" (i.e. form-specific at phase borders) interaction of space-like matter, celestial objects at various scales build up quantized fields of these forms of matter around their centers' of gravity of normal matter which reach far beyond the observable surface of such objects, respectively. From the description of the space-like matter fields of the Sun and the Earth a quantitative explanation of the reported NASA spacecraft anomalies of Pioneer 10 and 11 as well as of NEAR-Shoemaker at its fly-by maneuver on 01/23/1998 at Earth is given. The structure of such quantized subtle matter fields of stars allow in addition a description of the formation of "normal" and "inverse" planetary nebulae at the end of a star's life. - So-far unknown physical force-effects between subtle matter fields, bound, due to the topological interaction, at various metals were observed. The results allow an explanation of the at present relatively large uncertainty $\Delta G/G$ in the determination of Newton's constant of gravity. Devices for a more precise and reproducible determination of G (with an accuracy comparable to that of Planck's quantum of action, for example) should be made of beryllium or aluminium/beryllium alloy to eliminate subtle matter effects or such effects should be taken into account by a comprehensive theoretical modeling of their material and shape (and also to some extend time and place) depending force actions. Thus, both anomalies, the reported NASA spacecraft acceleration anomalies in the solar system as well as gravity anomalies at laboratory scale result from force-effects due to at present unknown subtle matter fields (of dark matter and of dark energy) bound at a cosmic scale to celestial objects and at a macroscopic scale to metals.

Keywords: dark matter, dark energy, spacecraft anomalies, gravity anomalies, planetary nebulae
PACS: 91.10.Op, 91.10.Sp, 95.35.+d, 95.36.+x, 98.38.Ly

ACCELERATION ANOMALIES OF NASA SPACECRAFT

Recently, a so-far unknown form of invisible, field-like, i.e. space-like, and quantized matter with real and weighable mass content was detected [1]. Using automatically working balances (Sartorius C 1000 or M25D-V two pan balance) with a reproducibility of $\pm 1\ \mu g$ the observed quanta exhibit Planck mass $m_P = \pm\sqrt{\hbar \cdot c/G} = \pm 21.77\,\mu g$, i.e. with positive or negative sign, as **candidates for dark matter and dark energy**. The quanta can form associations, as the experiments reveal. Usually, objects with

CP1166, *Sources and Detection of Dark Matter and Dark Energy in the Universe*, edited by D. B. Cline

Planck mass m_P are considered as **primordial black holes** generated in an early stage of the universe. This implies the assumption that Planck mass m_P is confined within a sphere of Schwarzschild radius $R_S = 2 \cdot m_P \cdot G/c^2 = 2 \cdot l_P$, where l_P is the Planck length $l_P = \sqrt{\hbar \cdot G/c^3} = 1.62 \cdot 10^{-35}$ m, yielding a density of $\rho = 3 \cdot m_P/(32 \cdot \pi \cdot l_P^3) = 1.41 \cdot 10^{95}$ kg/m^3, with expected rapid decay due to Hawking radiation. However, from synergistic superposition effects of neighboring samples which both had absorbed quanta of subtle matter at laboratory scale (see below) it could be deduced that subtle matter is characterized by a spatially extended field-structure ranging over distances of centimeters with a density of $\rho \leq 10^{-3}$ kg/m^3, and being stable in the course of time.

Celestial bodies absorb quanta of subtle matter due to their gravitational or topological interaction, yielding stationary fields of subtle matter superimposed to normal matter which range beyond the surface of a celestial object, respectively. The bodies of normal matter and field-like matter can be described as a quantized two-body system, where the subtle matter field with mass M_F is bound as a stationary wave-like structure around the celestial object of normal matter with mass M_C, by applying the following equations (1) through (7) where $t_P = l_P/c$, i.e. Planck time.

$$\Delta E_P \cdot \Delta t_P = m_P \cdot c^2 \cdot t_P = \hbar \tag{1}$$

$$(\Delta E_P)_N \cdot \Delta t_P = N \cdot m_P \cdot c^2 \cdot t_P = N \cdot \hbar,\ N = number\ of\ quanta\ per\ orbital \tag{2}$$

$$-(N^2 \cdot \hbar^2/(2 \cdot \mu)) \cdot \Delta\psi - G \cdot M_F \cdot M_C \cdot \psi/r + T(\psi^2) = E \cdot \psi \tag{3}$$

$$\psi_{1,0,0} = \psi(1s) = \sqrt{\pi} \cdot a_F^{-3/2} \cdot e^{-r/a_F} \tag{4}$$

$$\psi_{2,0,0} = \psi(2s) = (4 \cdot \sqrt{2 \cdot \pi})^{-0.5} \cdot a_F^{-3/2} \cdot (2 - r/a_F) \cdot e^{-r/(2 \cdot a_F)} \tag{5}$$

$$A(r,1s) = G \cdot M_{F1} \cdot [1 - (2 \cdot r^2/a_F^2 + 2 \cdot r/a_F + 1) \cdot e^{-2 \cdot r/a_F}]^p/r^2 \tag{6}$$

$$A(r,2s) = G \cdot M_{F2} \cdot [1 - (r^4/(8 \cdot a_F^4) + r^2/(2 \cdot a_F^2) + r/a_F + 1) \cdot e^{-r/a_F}]^p/r^2 \tag{7}$$

Equation (2) results as an extended Heisenberg uncertainty relation from (1) and yields a quantum of action $N \cdot \hbar$ for a boson-ensemble of N quanta of subtle matter with Planck mass m_P bound to a celestial body. (2) leads to a Compton wave of the absorbed boson-associate, according to $\lambda_{NC} = N \cdot \hbar/(M_F \cdot c)$, to which the de Broglie wave $\lambda_N = N \cdot \hbar/(M_F \cdot v)$ can be associated. This allows the formulation of the Schroedinger equation (3) for the two-body system of subtle matter bound in a cosmic orbital around a celestial object, with the reduced mass $\mu = M_F \cdot M_C/(M_F + M_C) \approx M_F$, where Δ in (3) is the Laplace operator. With the approximation $T(\psi^2) = 0$ for the non-linear term in (3), cosmic eigenvalues $E_n = -2 \cdot \pi^2 \cdot G^2 \cdot M_C^2 \cdot M_F^3/(n^2 \cdot N^2 \cdot h^2)$ result. With the radial distribution functions $P(r,\psi) = 4 \cdot r^2 \cdot \psi^2$, the radius dependent mass contents $M_F(r,\psi) = M_F \cdot \int_0^r P(r,\psi) \cdot dr$ of "**cosmic orbitals**" are obtained with the "cosmic Bohr radius" $a_F = N^2 \cdot h^2/(4 \cdot \pi^2 \cdot G \cdot M_F^2 \cdot M_C)$. Finally, distance dependent accelerations result from $A(r,\psi) = ((G \cdot M_F)/r^2) \cdot \int_0^r P(r,\psi) \cdot dr$, caused by such orbitals acting gravitationally on spacecraft in addition to the known gravitational accelerations, where M_F, N and p are adjustable parameters per orbital for the description of observed acceleration anomalies. By equations (6) and (7), for example, such additional accelerations can be calculated for the lowest eigenstates $\psi_{1,0,0}$ and $\psi_{2,0,0}$. The factor $p \geq 1$ steepens the obtained wave functions as a correction for the neglected term $T(\psi^2)$ in (3). Furthermore, a bosonic

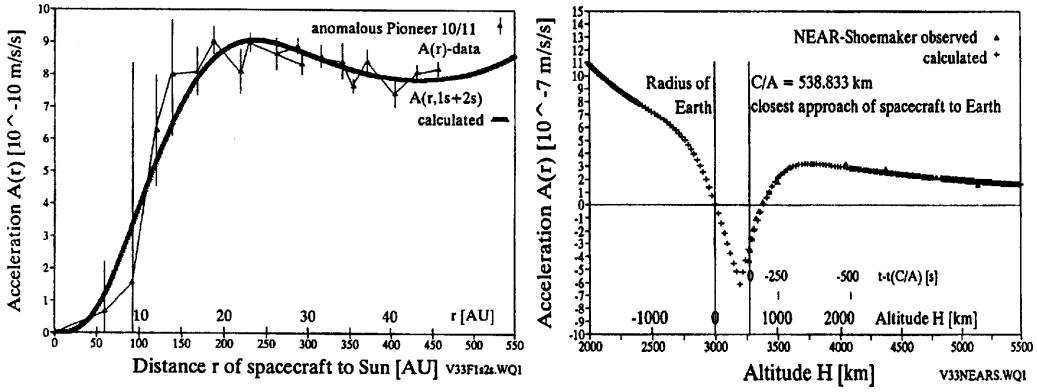

FIGURE 1. Pioneer 10/11 (left) and NEAR-Shoemaker (right) spacecraft acceleration anomalies.

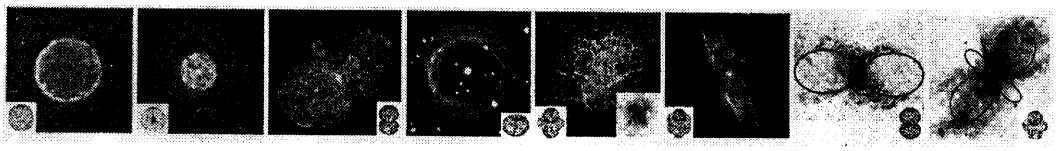

FIGURE 2. Examples of "normal" planetary nebulae, structured by $+m_P$-orbitals, respectively, are depicted in the first six Figures; from left to right: $1s$-orbital (Abell 39), $2s$ (IC 3568), $2p$ (Eta Carina), $2p^2$ (AAT 95), $3d_{z2}$ (crab nebula, central $3d_{z2}$-orbital shown as inset), $4f_{z3}$ (M2-9). Two examples of "inverse" planetary nebulae, structured by $-m_P$-orbitals, are shown in the last two Figures; left: 2p (spider nebula), right: $3d_{z2}$ (butterfly nebula). In these Figures non-visible, yet existing orbital lobes are indicated by ellipses. Also the owl nebula with a $2p(-m_P)$-structure belongs to the group of inverse nebulae.

distribution of quanta of subtle matter within an orbital is assumed, and a fermionic one between orbitals, as well as a $(1/r^2)$-force-law for the topological interaction. The results for simulations of the observed **NASA spacecraft acceleration anomalies of Pioneer 10/11 and NEAR-Shoemaker** [2] are given in Figure 1. The following parameters were used: solar-1s-orbital for $+m_P$-quanta with $M_F(1s) = 10^{27}$ kg, $N(1s) = 2.30 \cdot 10^{77}$, p = 1.8; solar-2s-orbital for $+m_P$-quanta with $M_F(2s) = 2.53 \cdot 10^{28}$ kg, $N(2s) = 4.4 \cdot 10^{78}$, p = 1.8; global-1s-orbital for $+m_P$-quanta with $M_F(1s) = 3.125 \cdot 10^{17}$ kg, $N(1s) = 5 \cdot 10^{61}$, p = 1; global-$2p^3$-shell-structured-orbital (bound by topological interaction, simulated as Gaussian curve) for gravitatively repulsive acting $-m_P$-quanta with $M_F(2p^3) = -1.46 \cdot 10^{18}$ kg, $r_0 = 6.75 \cdot 10^6$ m, $\sigma = 4.8 \cdot 10^5$ m. In both cases the simulated results fit well with the observed acceleration anomalies.

Explosive gas clouds at the end of a star's lifetime can be gravitationally attracted or rejected by $\pm m_P$-orbitals bound to the original star and its remnant, respectively, giving structure to the ejected material, leading to shapes of "**normal**" **planetary nebulae**, according to $+m_P$-orbitals, or "**inverse**" **planetary nebulae**, due to gravitatively repulsive effects of $-m_P$-orbitals (i.e. of dark energy), if a great amount or at least a part of the explosive cloud exhibits an explosion energy E_{exp} which is comparable with the gravitational energy E_{grav} of the bound orbitals, i.e. $E_{exp} \geq E_{grav}$, see Figure 2.

In galaxies $1s(+m_P)$-orbitals (i.e. of dark matter) of galactic size lead to the observed

anomalous rotation curves of galaxies, as simulations reveal, using velocity distributions, according to $V(r) = \sqrt{G \cdot M_C(r)/r + r \cdot A(r, 1s)}$, with $A(r, 1s)$ given by (6).

In universally widely distributed $3d_{z^2}$-orbitals (see Figure 2) of $+m_P$-quanta bound at celestial objects of various scale (i.e. at stars, black holes, quasars or galaxies, for example) the gravitational pull of the two centers of mass of the two orbital lobes in the rotation axis which are located perpendicular to the ring-shaped orbital cause the generation of **bipolar jet streams** of normal matter, away from the object, in opposite directions along the rotational axis of the system, see reference Nr. 4 in [1].

ANOMALIES OF NEWTON'S GRAVITY CONSTANT

Due to the topological, i.e. form-specific, interaction of field-quanta of subtle matter, metals or minerals with internal ionic lattice structures also absorb quanta of field-like matter and build up macroscopic fields of this form of matter which reach beyond their surface, respectively. The superposition of such two subtle matter fields, bound to metals/minerals, leads to weighable mass changes, due to resulting force-effects. This was observed when to one of two identical test samples suspended to the two arms of the two pan balance another metallic sample was approached and removed again after some time, see Figure 3 and Figure 4. As the experiments reveal, such distance-dependent force-effects are furthermore dependent on the composition and shape of the materials used (see Figure 4), and can also vary to some extend in time and also space. This implies that the usually accepted time- and space-independent reproducibility of physical experiments due to the assumed homogeneity of time (invariance of energy) and space (invariance of momentum) can be violated. The results explain why in tests for the determination of Newton's constant of gravity G non-reproducible results with large uncertainties regarding the value and variance of G were reported [3]. As can be seen from Figure 4, devices for a precise and reproducible determination of G should be made of beryllium or beryllium/aluminium alloy, to avoid such so-far unknown and therefore uncontrolled force effects due to the interaction of subtle matter fields bound to the frame as well as to the test samples in devices used for the determination of G.

DISCUSSION AND CONCLUSIONS

The presented results reveal that the observed Pioneer 10/11 and NEAR-Shoemaker **spacecraft anomalies** the reported **uncertainties in the determination of Newton's gravity constant**, as well as **structures of planetary nebulae** and **bipolar jet formation** can be explained on the basis gravitational actions of subtle matter fields, i.e. dark matter and dark energy, bound to normal matter by interactions found at laboratory scale.

In addition, the exponential terms in (6) and (7) lead with $n_i = 1, 2$ and the approximation $e^{-2 \cdot r/(n \cdot a_F)} \approx (1 - 2 \cdot r/(n \cdot a_F))$, due subtle matter fields bound to normal matter, to an extension of the law of gravity, i.e. to $F = G \cdot m_1 \cdot m/r^2 \pm \Sigma_i 2 \cdot G \cdot M_F(r)_i \cdot m/(n_i \cdot a_F \cdot r) + (terms\ of\ higher\ order\ of\ r,\ including\ M_F(r)_i/M_F(r)_j - interactions)$ for $r \ll a_F$, yielding an existing, yet hard to verify (in a reproducible way, see above), and gravitationally acting "**universal $M_F(r)$-fifth force**" in superposition with "**local $M_F(r)$-fifth-**

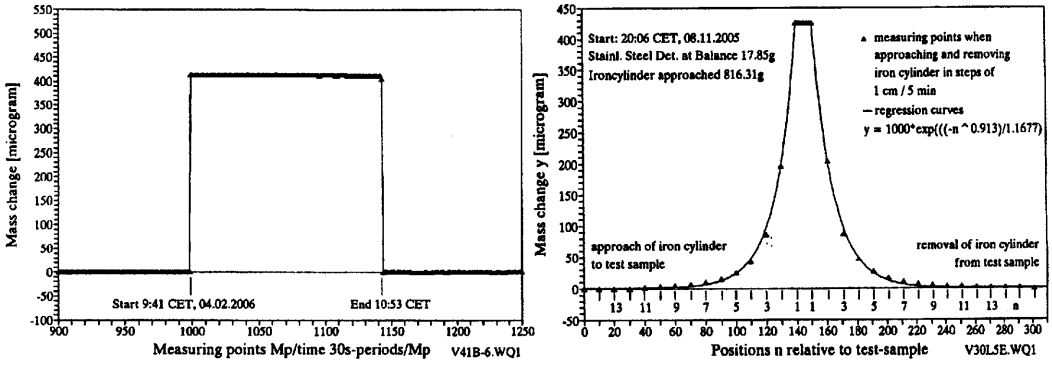

FIGURE 3. Left: To a non-magnetizable, prior to the test electrically grounded circular stainless steel plate (i.e. "detector", 17.85 g, diameter about 3.3 cm, thickness 0.2 cm) at the two pan balance (with an identical reference sample) a grounded iron cylinder (i.e. "heavy sample", 816.31 g, diameter 5.2 cm, hight about 4.9 cm) was approached from a distance of about 15 cm to a distance of about 5 mm within about 5 sec (without mechanical disturbance), and was removed again after 72 min within about 5 s. When approaching or removing the iron cylinder to the detector, the detector's mass reversibly changed, due to interaction of the two fields of subtle matter absorbed by the samples, respectively. Right: Same test, however with approaching and removing the iron sample in steps of 1 cm within 5 min, each.

Sample appr. / Detector	$_{13}$Al 273.89 g	$_{26}$Fe 816.31 g	$_{26}$Fe-Cr-Ni 763.51 g	$_{29}$Cu 873.12 g	$_{29}$Cu-Zn 831.96 g	$_{80}$Hg 250 g	$_{82}$Pb 912.35 g
$_{13}$Al 17.18 g	-/+0.3 µg	0.0 µg	+/- 0.2 µg	-/+0.6 µg	-/+0.5 µg	-/+0.5 µg	0.0 µg
$_{26}$Fe 19.35 g	+/- 1.3 µg	+/- 180 µg p≪0.00001	-/+ 112 µg p≪0.00001	+/- 0.5 µg	+/- 0.5 µg	-/+0.8 µg	-/+0.8 µg
$_{26}$Fe-Cr-Ni 17.85 g	+/- 0.3 µg	+/- 426 µg p≪0.00001	+/- 0.8 µg	0.0 µg	0.0 µg	-/+0.7 µg	+/- 0.8 µg
$_{29}$Cu 19.18 g	+/- 1.2 µg	+/- 0.5 µg	+/- 1.0 µg	+/- 2.0 µg p<0.001	+/- 1.2 µg	+/- 0.5 µg	+/- 1.2 µg
$_{29}$Cu-Zn 18.47 g	+/- 0.8 µg	+/- 0.9 µg	+/- 1.4 µg	+/- 1.1 µg	-/+0.5 µg	0.0 µg	+/- 0.2 µg
$_{82}$Pb 17.53 g	+/- 2.6 µg p<0.001	+/- 1.8 µg p<0.001	+/- 3.9 µg p<0.001	+/- 1.3 µg	+/- 2.6 µg p<0.001	+/- 0.2 µg	+/- 1.8 µg p<0.001

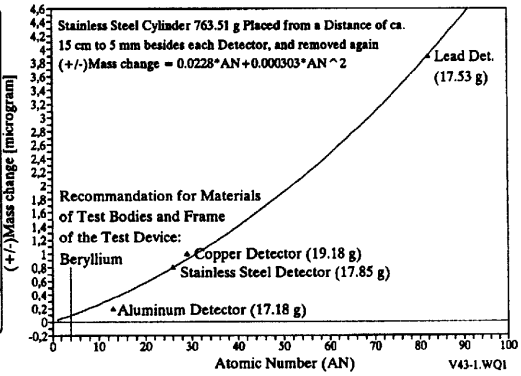

FIGURE 4. Left: Results obtained in tests as described in Figure 3 with various metals. The measured mass changes could be positive or negative, as indicated by +/- or -/+ in front of the measured effects, and were independent of approaching the heavy sample above, besides or below the respective detector. Right: Dependence of the observed mass changes by using the stainless steel sample (763.51 g) and various metal detectors as function of the atomic number of the detector's material, neglecting the strong effect between the stainless steel sample and the iron detector, see left Table.

force-effects", resulting from subtle matter fields of the solar system (see, for example, Figure 1, left), or emerging from subtle matter fields at Earth (see Figure 1, right, as well as Figure 3 and Figure 4). Such global force-effects may slightly vary from place to place, due to the composition of the local geological surroundings and the choice of the materials used for the construction of test devices, built to detect effects of a "fifth force". The presented considerations confirm the existence of a "(1/r)-**fifth force**" and also explain its controversial discussion some decades ago in scientific literature, see [4].

Furthermore, from $\pm\Sigma_i G_i' \cdot M_F(r)_i \cdot m/r$ in F follows for $r \gg a_F$ an average gravitational (a/r)-force acting from all subtle matter fields $M_F(r)_i$ bound to celestial objects (especially from dark matter, i.e cosmic $+(m_P)$-orbital-fields) at any universal mass m (Mach-Principle). It can be shown that this leads to a resulting force $F_I = a \cdot m \cdot [(4 \cdot \pi/3) \cdot G \cdot \rho_U \cdot R_U^2/c^2]$ acting at every universal mass m, causing the inertia of m, and thus **causing inertia of any form of matter** [5], as described by Newton's second axiom. ρ_U in $[(4 \cdot \pi/3) \cdot G \cdot \rho_U \cdot R_U^2/c^2]$ is the average universal density $\rho_U \approx 9.5 \cdot 10^{-27}$ kg/m^3, and $R_U = c \cdot T_U = 1.3 \cdot 10^{26}$ m is the universal radius, yielding $[(4 \cdot \pi/3) \cdot G \cdot \rho_U \cdot R_U^2/c^2] \approx 0.5$. However, it can be shown that from the equation of definition $\rho_U = 3 \cdot M_U/(4 \cdot \pi \cdot R_U^3)$ and the assumption that the Universe can be considered as being a black hole (with internal flat space-time [6]) with Schwarzschild radius $R_U = 2 \cdot M_U \cdot G/c^2$, it follows by elimination of M_U from both equations that $2 \cdot [(4 \cdot \pi/3) \cdot G \cdot \rho_U \cdot R_U^2/c^2] \equiv 1$ must hold. Thus, the consistency of the considerations leads to the conclusion that the **Universe represents a black hole**.

Finally, a cosmic back ground radiation of field-quanta of subtle matter with positive sign exists, emitted, for example, from all stars in the Universe which transfers real momentum to normal matter, see the results from sun eclipse experiments in [1]. The presented results depicted in Figure 3 and Figure 4 indicate that the same flux of cosmic back ground radiation with constant intensity I_R also transfers real momentum on subtle matter fields bound for example to metals. This is consistent with an explanation that in a macroscopic quantum mechanical symmetric superposition of two metal bound subtle matter fields of two neighboring pieces of metal an enlargement of every individual field occurs. In this case the cross section area of any of the two fields is extended, resulting in an increased transfer of momentum from the mentioned back ground radiation to any of the two samples. A symmetrical superposition should therefore lead to weight increases of detectors suspended to the balance when another piece of metal is approached, as observed, see Figure 3. On the other hand, an anti-symmetrical overlap of the two fields of a pair of samples reduces the individual extension of every field. This should result in a reduced weight of a detector, again as observed. According to these interpretations of the results, given in the Table of Figure 4, both effects are consistent with a mechanism of gravity, according to "**Le Sage Gravity**", in accordance with Einstein's GTR, where space-time bending leads to an increase of the flux-density of the mentioned back ground radiation and thus causes increasing gravity-effects. These considerations allow a deepened understanding why, according to GTR, space-time curvature is correlated to the generation of gravity effects, for further details see [7].

REFERENCES

1. K. Volkamer, *Nuclear Physics B (Proc. Suppl.)* **124**, 127–127 (2003).
2. J. D. Anderson, *Phys. Rev. D* **65**, 082004–082057 (2002).
3. F. Nolting, *Europhysics News* **31**, 25–27 (2000).
4. E. Fischbach, and C. Talmadge, *Nature* **356**, 207–215 (1992).
5. J. Orear, *Physik*, Carl Hanser Verlag, München, 1991, pp. 472–472.
6. C. Brans, and R. H. Dicke, *Phys. Rev.* **124**, 925–935 (1961).
7. K. Volkamer, *Feinstoffliche Erweiterung unseres Weltbildes*, Weissensee Verlag, Berlin, 2008, pp. 167–270.

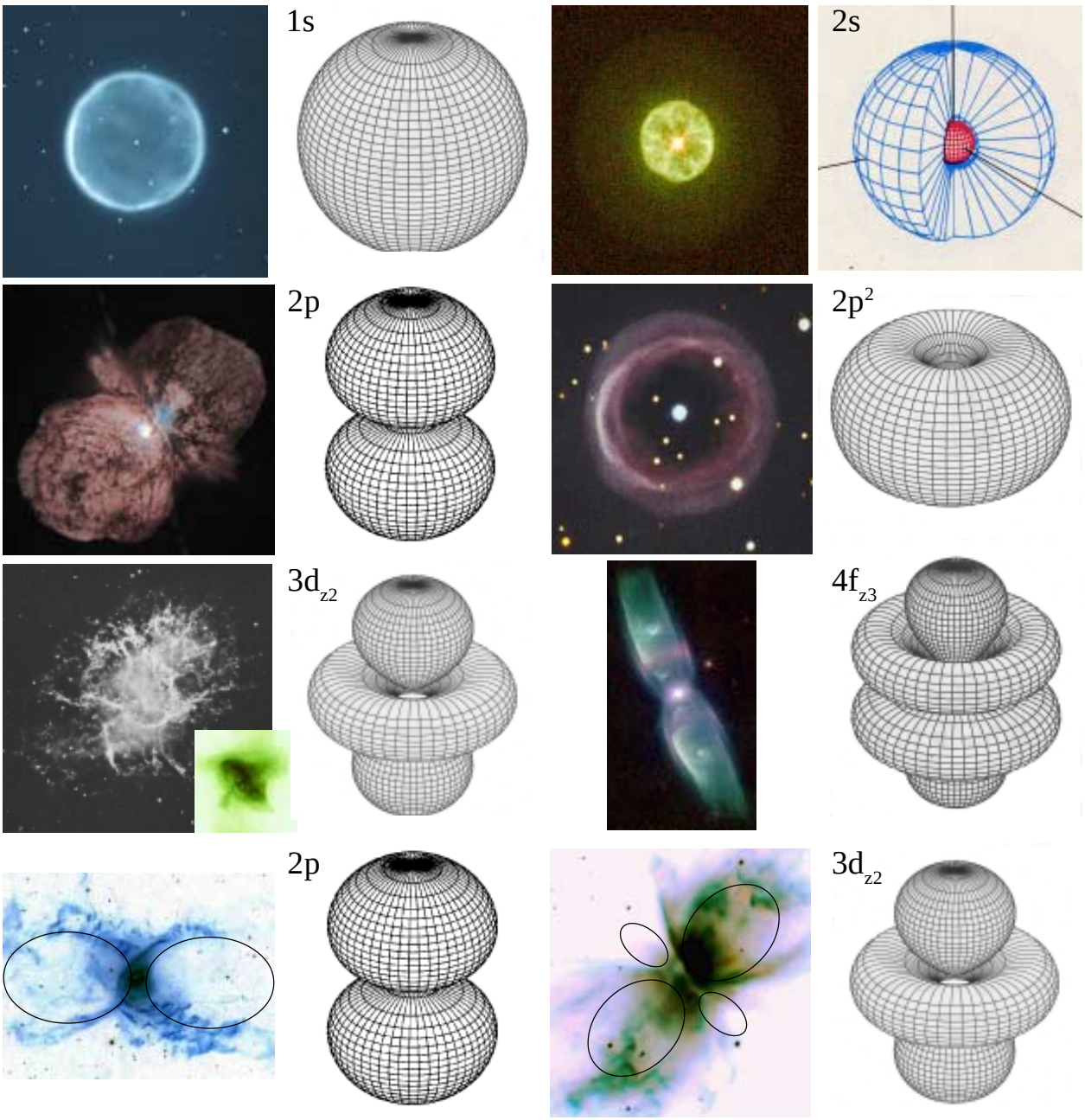

FIGURE 2. Examples of "normal" planetary nebulae, structured by $+m_p$-orbitals, respectively, are depicted in the first six Figures; from left to right: 1s-orbital (Abell 39), 2s-orbital (IC 3568), 2p-orbital (Eta Carina), $2p^2$-Ring-orbital (AAT 95), $3d_{z2}$-orbital (crab nebula, central $3d_{z2}$-orbital shown as inset), $4f_{z3}$-orbital (M2-9). Two examples of "inverse" planetary nebulae, structured by $-m_p$-orbitals, are shown in the last two Figures; left: 2p-orbital (spider nebula), right: $3d_{z2}$-orbital (butterfly nebula). In these Figures non-visible, yet existing orbital lobes are indicated by ellipses. Also the owl nebula with a $2p(-m_p)$-structure belongs to the group of inverse nebulae.